Noise characteristics with CMOS sensor array scaling

Measurement 152 (2020) 107325

Contents lists available at ScienceDirect

Measurement

journal homepage: www.elsevier.com/locate/measurement

Noise characteristics with CMOS sensor array scaling

Claudio Accarino [a,*,1], Valerio F. Annese [a,1], Boon Chong Cheah [a], Mohammed A. Al-Rawhani [a], Yash D. Shah [a], James Beeley [a], Christos Giagkoulovitis [a], Srinjoy Mitra [b], David R.S. Cumming [a]

[a] Department of Electrical and Electronic Engineering, University of Glasgow, Rankine Building, Oakfield Avenue, Glasgow G12 8LT, UK
[b] School of Engineering, University of Edinburgh, Edinburgh EH93FF, UK

ARTICLE INFO

Article history:
Received 4 April 2019
Received in revised form 8 August 2019
Accepted 25 November 2019
Available online 27 November 2019

Keywords:
Semiconductor device noise
Noise measurement
CMOS
Ion-sensitive field effective transistor (ISFET)
Photodiode
Single Photon Avalanche Diode (SPAD)

ABSTRACT

An important consideration when scaling semiconductor sensor devices is the effect it may have on noise performance. Overall signal to noise ratio can be improved both by increasing sensor size, or alternatively by averaging the signal from two or more smaller sensors. In the design of sensor systems it is not immediately clear which is the best strategy to pursue. In this paper, we present a detailed theoretical and experimental study based on three different sensor arrays that show that an array of small independent sensors is always less noisy than a large sensor of the same size.

1. Introduction

Complementary metal oxide semiconductor (CMOS) technology has enabled mass production of large arrays for applications from imaging [1] to genomics [2]. Typically, sensors shrink in size as technology scales to smaller geometry [3,4]. As sensors become smaller the signal-to-noise-ratio (SNR) diminishes because of phenomena including reduced optical aperture for image sensors, or reduced available reagent volume and surface area for biological sensors. This is because in many cases, the noise is set by the shot-noise limit that cannot improve as the sensor signal becomes smaller [5–8].

In this article, we consider the question of whether for sensing application the overall SNR is best improved by using fewer, larger area sensors, or by averaging the signal from more independent smaller sensors in an array configuration. Temporal averaging uncorrelated signals has been already proved to increase the SNR [9,10]. Temporal image averaging is a reliable and robust method for quality and SNR enhancement [11], particularly suited for high noise and low sensitivity applications [12,13].

On the contrary spatial average of uncorrelated non-image signal on sensor arrays is a relatively unexploited field. Work in [14,15] demonstrated a reduction of the mean square (MS) noise as a function of the square root of the average number of sensors using a 256 × 256 array of ion sensitive field effect transistors (ISFET) and a 16 × 16 array of photodiodes, respectively. In order to develop a consistent theory in support of sensor array design we present a theoretical and experimental analysis of three different arrays of sensors: a 256 × 256 ISFET array, a 32 × 32 array of Single Photon Avalanche Diode (SPAD) and a 16 × 16 PD array. We show that an array of small independent sensors performs better than a single large sensor, regardless of the nature and the origin of the noise in the sensor. Moreover, this approach may be used to optimize lab-on-chip and micro-fluidic design when multiple assays are to be performed on one array.

2. Theoretical analysis

In this section any quantity with the subscript 'A' refers to an array of sensors whilst the subscript 'B' denotes a large single sensor.

2.1. Array of sensors

An array of M independent sensors (or pixels) having a single output obtained by spatial and temporal averaging is considered. We assume that for each sensor in array, numbered i, the noise $n_i(t)$ is additive and uncorrelated to the signal $s_i(t)$, as shown in

* Corresponding author. University of Glasgow, UK
E-mail address: c.accarino.1@research.gla.ac.uk (C. Accarino).
[1] Both authors contributed equally to this work.

https://doi.org/10.1016/j.measurement.2019.107325
0263-2241/

Fig. 1(a). The noise is also assumed to be uncorrelated between different sensors. The noise originating from a CMOS chip, n(t), may be divided into three different components based on their mechanism of action and properties: thermal noise, flicker noise and shot noise [16]. Since these noise components have different origin, they will be independent, and the mean square (MS) voltage of the noise, e_n^2, can therefore be written for a data sample in an arbitrary interval of time Δt as:

$$e_n^2 \overset{\text{def}}{=} \frac{1}{\Delta t}\int_{\Delta t} n^2(t) \overset{\text{def}}{=} e_{ther}^2 + e_{fli}^2 + e_{shot}^2 \tag{1}$$

The time dependent output function $v(t)$ obtained for each sensor is therefore $v_i(t) = s_i(t) + n_i(t)$ thus, since the signal and noise are uncorrelated $v_i^2(t) = s_i^2(t) + n_i^2(t)$. The MS voltage noise, e_A^2, for an array of independent sensors calculated on a data sample in an arbitrary interval of time Δt, is given as:

$$\begin{aligned} e_A^2 \overset{\text{def}}{=} \frac{1}{\Delta t}\int_{\Delta t} v_A^2(t)dt &= \frac{1}{\Delta t}\int_{\Delta t}\frac{1}{M}\sum_{i=1}^{M} v_i^2(t)dt \\ &= \frac{1}{\Delta t}\int_{\Delta t}\frac{1}{M}\left(\sum_{i=1}^{M} s_i^2(t) + \sum_{i=1}^{M} n_i^2(t)\right) \\ &= \frac{1}{M}\left(\frac{1}{\Delta t}\int_{\Delta t} s_A^2(t)dt + \frac{1}{\Delta t}\int_{\Delta t} n_A^2(t)dt\right) \\ &= \frac{1}{M}\left(e_{sA}^2 + e_{nA}^2\right) = \left(\frac{e_{sA}}{\sqrt{M}}\right)^2 + \left(\frac{e_{nA}}{\sqrt{M}}\right)^2 \end{aligned} \tag{2}$$

where $s_A^2(t) \overset{\text{def}}{=} \sum_{i=1}^{M} s_i^2(t)$ and $n_A^2(t) \overset{\text{def}}{=} \sum_{i=1}^{M} n_i^2(t)$.

2.2. Single sensors

If we consider a single sensor with an area equivalent to the total area of the aforementioned array (A_B = M*A_A), and assume additive noise as before, the following expression for an equivalent single sensor as shown in Fig. 1(b) is obtained:

$$v_B^2(t) = s_B^2(t) + n_B^2(t) = \frac{s_A^2(t)}{M} + n_B^2(t) \tag{3}$$

The MS voltage noise for the single sensor, analogous with (2), is given by:

$$e_B^2 = e_{sB}^2 + e_{nB}^2 = \left(\frac{e_{sA}}{\sqrt{M}}\right)^2 + e_{nB}^2 \tag{4}$$

2.3. Free noise signal comparison

Comparing (2) with (4), we see that the pure signal from both the single sensor and the array of sensors are the same whereas, the noise component is not. Based on the three independent noise components defined in (1), it can be proved that the following relationships exist between a single sensor and the averaged array:

$$e_{fli_A}^2 \cong e_{fli_B}^2; e_{ther_A}^2 \cong e_{ther_B}^2; e_{shotA}^2 = e_{shot\_B}^2 \tag{5}$$

Therefore, the following relationship may be derived:

$$e_{nB}^2 \cong e_{ther_A}^2 + e_{fli_A}^2 + e_{shot_A}^2 = e_{nA}^2 \tag{6}$$

By combining (2), (4) and (6) it can be concluded that:

$$\frac{e_A^2}{e_B^2} \cong \frac{\left(\frac{e_{sA}}{\sqrt{M}}\right)^2 + \left(\frac{e_{nA}}{\sqrt{M}}\right)^2}{\left(\frac{e_{sA}}{\sqrt{M}}\right)^2 + e_{nA}^2} = \frac{1}{M} \tag{7}$$

This result is perfectly in line with the Gaussian statistics expected from the noise components and the work in [7]. To verify the validity of our theoretical analysis, experimental measurements were performed on sensor microarrays.

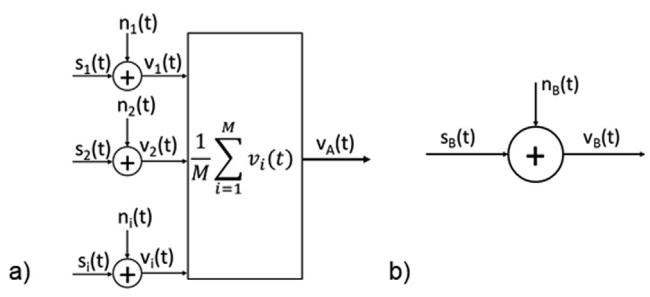

Fig. 1. (a) Block diagram of the averaging process on an array of sensors. (b) Single sensor output.

3. Experimental results

3.1. Sensors and systems

We conducted experiments on 3 different arrays of sensors: a 256 × 256 ISFET array chip [14], a 16 × 16 photodiode (PD) array chip [15], a 32 × 32 SPAD array chip [17] illustrated in Fig. 2(a)–(c) respectively.

The 256 × 256 ISFET sensor array chip was fabricated using the standard AMS 0.35 μm four metal process. With a pixel size of 10. 2 μm × 10.2 μm, the entire array occupies an area of approximately 2.87 mm × 2.87 mm. The device employed was also post-processed with a layer of Ta2O5 which increased the sensitivity of the sensors and reduced the time-drift. The 256 × 256 ISFET sensor array chip has been described in related works [14].

The 16x16 PD array chip was fabricated with 0.35 μm CMOS process provided by Austriamicrosystems. The photodiode pixel measured 10 μm × 24 μm and the size of the entire chip was 3.4 mm × 3.6 mm. More details about this chip has been reported in a different work [15].

The 32 × 32 SPAD array chip was fabricated in an AMS 0.35 μm high voltage mixed signal triple-well CMOS process. The size of the chip was 3.7 mm × 3.7 mm and integrates SPAD pixels, a controllable charge pump, read-out circuitry and 32 × (16-bit) digital pulse counters. The SPAD array has been presented in a correlated work [17].

Prior to performing measurements, the array chips were packaged with an encapsulation sealant for protecting the bond pads and wire bonds. The packaging recipe has been described in related works [14]. In order to operate the array chips, a printed circuit board (PCB) platform was designed to integrate the chips with an ARM mbed STM32 Nucleo-F334R8 board (STMicroelectronics, UK). The mbed performed addressing, data digitization and data transfer via USB to a PC where a MATLAB software displayed, acquired and saved data.

3.2. Experimental setup and sub-arrays organization

To mimic arrays with different number of pixels and analyze the results, the signals from the experimental arrays were organized into sub-arrays. The signal from each pixel was assumed to give rise to random ergodic noise. To eliminate temporal variation, we collected our data from the full array for 1 min at the maximum possible frame rate of the system, corresponding to 10, 14, and 3 fps for ISFET, PD, and SPAD respectively. The collected data were averaged pixel by pixel for all frames. Complete datasets for whole arrays were post-processed using MATLAB. Virtual sub-arrays were

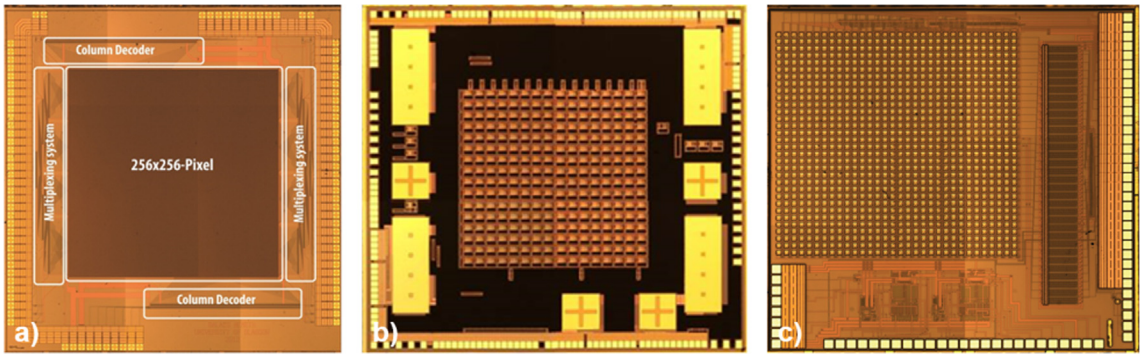

Fig. 2. (a) The 256 × 256 ISFET chip, (b) the 16x16 PD chip, and (c) the 32 × 32 SPAD chip.

formed by randomly choosing pixels from the full array. On the three arrays studied, the smallest had only 256 pixels. In order to be consistent virtual sub-arrays of 2 up to 256 pixels were therefore evaluated, even in those devices where larger arrays were available. Virtual sub-arrays were composed by randomly selecting pixels across the arrays of 256 pixels. Pixels for each sub-array were selected in code, and the sub-arrays were combined in a virtual array having a total of 256 pixels. The data analysis was performed 10 times with different random selections in each case to minimize the impact of bias and error. Each virtual array was statistically characterized in terms of standard deviation, variance and mean values.

A simplified pseudo-code, showing how Matlab generated sub-arrays and randomly assign pixels to each sub-arrays, is reported in below. Commands are highlighted in bold; variable are shown in italics and comments are reported in green colour after a percentage symbol. The first and last command of the pseudo-code are written in capital letter to mark the beginning and the end of the pseudo-code. Since the illustrated pseudo-code is written for one array at a time, it is required to be run three times.

```
BEGIN
For i1:=1 to 10, step + 1 do
  Sample_population = randomly selected 256 pixels from
  array_population;
  % select 256 pixels from the array population
  For i2:=0 to 8, step + 1 do % for loop, from 0 to 8 with a pace
  of 1
    n_sub-arrays = 2^i2; % calculate the number of sub-arrays,
  which is equal to 2^i2
    n_pixels_sub-array = 256/(2^i2)
    % calculate number of pixels per sub-array
      For i3:=1 to n_sub-arrays, step + 1 do % for loop, from 1
  to n_sub-arrays with a pace of 1
      sub-array_i3 = 256/(2^i2) randomly selected pixels
  from Sample_population;
      % generate a sub-array and randomly assign 256/(2^i2)
  pixels
      end
  end
end
```

3.3. Experimental results

The histograms in Fig. 3(a)–(c) show the variance versus the number of pixels in a sub-array for the ISFET, PD, and SPAD arrays respectively. We applied non-linear regression to the bar plots and the fitting curve was found to be 1/M, with M being the number of averaged pixels on any array. The data for two or more sensors can be fitted using the regression model to determine the noise in a single sensor if it was scaled in size by a factor M. The bar graphs show how a reduction of one order of magnitude of the variance value is easily achievable by dividing the one large sensor into 8 smaller sensors, occupying the same area overall. Scaling down to 128 sensors reduces the variance by another order of magnitude.

Based on this observation and on the experimental results reported in Table 1, it can be concluded that an array of sensors performs better than a single sensor. Moreover, as experimental results are consistent for each of the three arrays, regardless their sensing and noise mechanisms, we can assume the averaging process is sensor independent and therefore valid.

3.4. Discussion

Our findings demonstrate that there is merit of using a sensor array rather than a standalone sensor with the same area independently by the type of the sensor. When designing a sensing system, our findings mean that the designer has to be aware that - for a given application - it is possible to achieve a defined standard deviation by tuning the number of sensors embedded into the sensor array employed for the measurement. Therefore, any given sensor array as an intrinsic accuracy limit. Our findings show similar results to works where the overall SNR of an image was improved by temporal averaging [11–13] and spatial and temporal average on multiple separate acoustic sensor was implemented [10].

Additionally, our findings are relevant to spatial and temporal average on a single array of sensors; our results are particularly relevant when a sensor array is physically divided in several sensing areas to perform simultaneous sensing. The physical separation of the sensing area is usually achieved by the development of a microfluidic network – especially in lab-on-chip or point-of care applications. Our studies imply that the number of microfluidic channels into a network is limited not only by the fabrication technique but also by the required accuracy of the target measurement. In fact, given a fixed sensing area with a fixed number of sensors, increasing the number of channels imply a reduction of the size of the microfluidic channels and a reduction of the sensors dedicated to a single channel. Thus, each measurement taken from the microfluidic channel would have an increased dispersion. In summary, when comes to designing a microfluidic network on the top of a sensor array, the designer has to consider that the size of the microfluidic channel and the channel density within the network are linked to the dispersion of the target measurement.

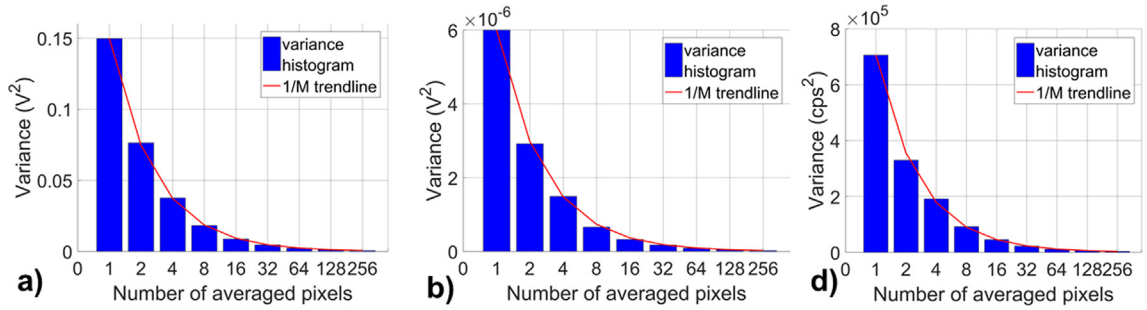

Fig. 3. Variances versus number of averaged pixels plot for (a) ISFET array, (b) PD array, and (c) SPAD array. Fitting curve is plotted in red. (For interpretation of the references to colour in this figure legend, the reader is referred to the web version of this article.)

Table 1
Experimental results of variance versus number of averaged pixels for ISFET, PD and SPAD.

Number of pixels	ISFET variance (V^2)	PD variance (V^2)	SPAD variance (cps^2)
1	0.1496	0.000006	705,957
2	0.076268769	2.91526E−06	329,476
4	0.037610381	1.49233E−06	190,969
8	0.018285733	6.60015E−07	91,809
16	0.008763422	3.22667E−07	44,944
32	0.004597231	1.75743E−07	22,500
64	0.002312726	8.73203E−08	11,449
128	0.001150784	4.35315E−08	5776
256	0.000573284	2.18E−8	2809

4. Conclusion

In this paper we have compared the noise performance of a sensor system made using a single large sensor, versus the noise achieved when averaging the signal from an array of small independent sensors. Whilst the SNR of a smaller physical sensor is typically less than that of a single larger sensor, the properties of uncorrelated Gaussian noise are such that the overall performance of an array of small sensors is significantly better when the signal is averaged.

This elegant result suggests that there is merit in using sensor arrays, such as those that can be implemented in CMOS, even if the application only calls for a single measurement. Given the relatively low cost of CMOS and the wide availability of CMOS sensors, it is therefore beneficial to use arrays in any application where low noise or multiple parallel sensing are a priority.

Declaration of Competing Interest

The authors declare that they have no known competing financial interests or personal relationships that could have appeared to influence the work reported in this paper.

Acknowledgement

This work was supported by EPSRC under grants EP/K021966/1, EP/L016753/1 and EP/N509668/1. The complete dataset can be found at the following link: http://dx.doi.org/10.5525/gla.researchdata.635.

References

[1] H. Rhodes et al., The Mass Production of Second Generation 65 nm BSI CMOS Image Sensors, Isw2011, pp. 1–6, 2011.
[2] J.M. Rothberg et al., An integrated semiconductor device enabling non-optical genome sequencing, Nature 475 (7356) (2011) 348–352.
[3] J.A. Richardson, E.A.G. Webster, L.A. Grant, R.K. Henderson, Scaleable single-photon avalanche diode structures in nanometer CMOS technology, IEEE Trans. Electron Devices 58 (7) (2011) 2028–2035.
[4] N. Moser, T.S. Lande, P. Georgiou, Scaling ISFET instrumentation with in-pixel quantisation to deep submicron technologies, in: Proc. - 2016 IEEE Biomed. Circuits Syst. Conf. BioCAS 2016, 2017, pp. 436–439.
[5] Y. Liu et al., "An Extended CMOS ISFET Model Incorporating the Physical Design Geometry and the Effects on Performance and Offset Variation," vol. 58, no. 12, pp. 4414–4422, 2011.
[6] B. Lakshmi, A parallel model for Noise reduction of images using smoothing filters and Image averaging, Indian J. Comput. Sci. Eng. 2 (6) (2011) 837–844.
[7] K.M. Findlater et al., Implementing a CMOS image sensor noise performance model, Int. Image Sens. Work. (2007) 47–50.
[8] M. Crescentini, M. Bennati, M. Carminati, M. Tartagni, Noise limits of CMOS current interfaces for biosensors: a review, IEEE Trans. Biomed. Circuits Syst. 8 (2) (2014) 278–292.
[9] O. Rompelman, H.H. Ros, Coherent averaging technique: a tutorial review Part 1: Noise reduction and the equivalent filter, J. Biomed. Eng. 8 (1) (1986) 24–29.
[10] J. Grythe, N. As, "Array gain and reduction of self-noise," no. 9, pp. 1–2, 2015.
[11] J.M. Boyce, Noise reduction of image sequences using adaptive motion compensated frame averaging San Francisco, CA, USA, in: [Proceedings] ICASSP-92: 1992 IEEE International Conference on Acoustics, Speech, and Signal Processing, 1992, pp. 461–464.
[12] Yazan M. Dweiri et al., Ultra-low noise miniaturized neural amplifier with hardware averaging, J. Neural Eng. 12 (2015) 046024.
[13] C.L. Kumaragamage, B.J. Lithgow, Z.K. Moussavi, Investigation of a New weighted averaging method to improve SNR of electrocochleography recordings, IEEE Trans. Biomed. Eng. 63 (2) (2016) 340–347.
[14] B.C. Cheah et al., An integrated circuit for chip-based analysis of enzyme kinetics and metabolite quantification, IEEE Trans. Biomed. Circuits Syst. 10 (3) (2016) 721–730.
[15] M.A. Al-Rawhani et al., A colorimetric CMOS-based platform for rapid total serum cholesterol quantification, IEEE Sens. J. 17 (2) (2017) 240–247.
[16] S. Sze, Physics of Semiconductor Devices, first ed., Wiley-Interscience, New York, 1969.
[17] M.A. Al-Rawhani, J. Beeley, D.R.S. Cumming, Wireless fluorescence capsule for endoscopy using single photon-based detection, Sci. Rep. 5 (1) (2016) 18591.